An analytical and computational study of the incompressible Toner-Tu Equations

John D. Gibbon[a], Kolluru Venkata Kiran[b], Nadia Bihari Padhan[b], Rahul Pandit[b]

[a]*Department of Mathematics, Imperial College London, London SW7 2AZ, UK*
[b]*Centre for Condensed Matter Theory, Department of Physics, Indian Institute of Science, Bangalore, 560012, India*

Abstract

We consider the incompressible Toner-Tu (ITT) partial differential equations (PDEs), which are an important example of a set of active-fluid PDEs. They share many properties with the Navier-Stokes equations (NSEs) but there are also important differences. The NSEs are usually considered either in the decaying or the additively forced cases, whereas the ITT equations have no additive forcing, but instead have a linear, activity term $\alpha\boldsymbol{u}$ (with $\boldsymbol{u}$ the velocity field), which pumps energy into the system; they also have a negative $\boldsymbol{u}|\boldsymbol{u}|^2$-term that stabilizes growth and provides a platform for either frozen or statistically steady states. These differences make the ITT equations an intriguing candidate for study using a combination of PDE analysis and pseudo-spectral direct numerical simulations (DNSs). In the $d = 2$ case, we have established global regularity of solutions. We have also shown the existence of bounded hierarchies of weighted, time-averaged norms of both higher derivatives and higher moments of the velocity field. For $d = 3$ there are equivalent bounded hierarchies for Leray-type weak solutions. We present results for these norms from our DNSs in both $d = 2$ and $d = 3$, and contrast them with their counterparts for the $d = 3$ NSEs.

Keywords: Active matter, Toner-Tu, Navier-Stokes, PDE

1. Introduction

The field of *active matter* continues to grow rapidly [1–25]. The term is generally used for systems that have bodies, e.g., *birdoids* in computer animations [1], birds in a flock [2, 4, 5], or bacteria in dense suspensions [4–17], all of which use some source of energy, typically internal, to move or to apply forces. Such bodies, referred to as *active particles* in the physics literature, mutually interact and lead to non-equilibrium states, which may display rich spatio-temporal evolution. The bird-flocking model of Vicsek [2], a non-equilibrium version of a Heisenberg-spin model, is defined in discrete time, for an assembly of point particles, which are distributed randomly in space; these particles try to align with their neighbours, but with some error that is modelled stochastically.

Soon after the development of the Vicsek model, Toner and Tu (TT) introduced a hydrodynamic stochastic partial differential equation (PDE) that models flocking phenomena [4, 5].

Email addresses: j.d.gibbon@ic.ac.uk (John D. Gibbon), kollurukiran@iisc.ac.in (Kolluru Venkata Kiran), nadia@iisc.ac.in (Nadia Bihari Padhan), rahul@iisc.ac.in (Rahul Pandit)

The TT velocity field obeys a generalised, compressible, stochastically forced Navier-Stokes (NS) equation, which is not Galilean invariant. Meanwhile, other hydrodynamic PDEs were developed to study the spatio-temporal evolution evolution of active fluids, such as dense bacterial suspensions [4–17], or *active nematics*. These PDEs are also related to the Navier-Stokes equations. In one of the simplest variants, called either the mean-bacterial-velocity or the Toner-Tu-Swift-Hohenberg (TTSH) model, a term, consisting of the sum of a negative Laplacian and a bi-Laplacian, is added to an incompressible, deterministic TT PDE (henceforth, ITT) [20]. For recent studies of the stochastically forced and deterministic variants of the ITT we refer the reader to Refs. [21–25].

Although these active-matter and active-fluid PDEs have been studied intensively over the past two decades from the perspective of physics, and the results of these investigations have been compared with their experimental counterparts, methods of PDE-analysis, which have commonly been used to study the Navier-Stokes equations [26–30], have rarely been applied to the ITT equations. An exception is the work of Zanger, Löwen, and Saal on the regularity of solutions of the TTSH equations [31]. It turns out that similar PDEs have been studied using the methods of analysis in the context of the NS equations with an absorption term [32] or the Brinkman-Forchheimer-extended Darcy model of porous media [32–44]. The major difference is that these models have a nonlinearity that breaks the NS-invariance enjoyed by the ITT equations. While numerical methods and experiments are able to track a solution that evolves from *specified* initial conditions, methods of analysis are unable to do this; instead, in a complementary fashion, they provide us with constraints on solutions that evolve from *all smooth initial conditions*. They also provide upper bounds on average inverse length scales, which can be interpreted as lower bounds on the grid sizes necessary to resolve solutions.

Keeping these things in mind, we have studied the d-dimensional ITT PDEs using the ideas developed in Refs. [45–48], where a combination of analysis and direct numerical simulations (DNSs) on the $d = 3$ Navier-Stokes equations was used to match the results of the former against those of the latter. As in Refs. [45–48], one should not expect the estimated bounds to be saturated as these take into account all smooth initial conditions, however large, in a periodic domain. The direct numerical simulations of the ITT equations in this paper in both $d = 2$ and $d = 3$ have been based on pseudo-spectral methods. In §2 we define the PDEs in dimensionless form and the quantities that are required for our analysis. In §3 the scaling properties of the Navier-Stokes and the ITT equations are discussed and how their similarity acts as a guide to our choice of moments of higher derivatives of the velocity field. In §4 we discuss energy estimates. In §5 we describe the pseudo-spectral DNS that has been used to solve the ITT equations. In §6 we present a summary of our results in the $d = 2$ case, and likewise for the $d = 3$ case in §7. In both cases, proofs have been relegated to the Appendices. In §8 we discuss the significance of our results and compare them with similar results for related PDEs.

2. Dimensionless equations

The standard form of the incompressible Toner-Tu (ITT) equations is given by [4, 5, 21] :

$$(\partial_t + \lambda \boldsymbol{u} \cdot \nabla)\, \boldsymbol{u} + \nabla p = \alpha \boldsymbol{u} + \nu \Delta \boldsymbol{u} - \beta \boldsymbol{u} |\boldsymbol{u}|^2 \,. \tag{2.1}$$

The fixed parameters α, β are positive and the velocity field $\boldsymbol{u}$ satisfies the incompressibility condition $\operatorname{div} \boldsymbol{u} = 0$. β has the dimension $TL^{-2} \equiv [\nu^{-1}]$, α is a frequency and λ is a dimensionless parameter. The domain is taken to be a periodic box $[0, L]^d_{per}$. We leave remarks until §3 on the literature involving generalizations of this system to a $\boldsymbol{u}|\boldsymbol{u}|^{2\delta}$ nonlinear term.

The first step is to introduce a typical velocity field U_0 for which we have two definitions:

$$U_0 = \sqrt{\alpha/\beta}\,; \qquad\qquad U_0 = \nu/L\,. \tag{2.2}$$

Then primed dimensionless variables are defined thus :

$$\boldsymbol{x}' = L^{-1}\boldsymbol{x}\,; \qquad t' = U_0 L^{-1} t\,; \qquad \boldsymbol{u}' = \lambda U_0^{-1}\boldsymbol{u}\,; \qquad p' = \lambda U_0^{-2} p\,. \tag{2.3}$$

This transforms (2.1) into the dimensionless ITT equations (dropping the primes) which, from now on, will be the form used in this paper :

$$\begin{aligned} (\partial_t + \boldsymbol{u}\cdot\nabla)\,\boldsymbol{u} + \nabla p &= \alpha_0\boldsymbol{u} + \mathrm{Re}_\nu^{-1}\Delta\boldsymbol{u} - \mathrm{Re}_\beta\,\boldsymbol{u}|\boldsymbol{u}|^2\,,\\ \mathrm{div}\,\boldsymbol{u} &= 0. \end{aligned} \tag{2.4}$$

These operate on the unit periodic box $V_d = [0, 1]^d$. The two Reynolds numbers Re_ν and Re_β are defined as follows :

$$\mathrm{Re}_\nu = \frac{U_0 L}{\nu}\,; \qquad \mathrm{Re}_\beta = \frac{\beta U_0 L}{\lambda^2}\,; \tag{2.5}$$

and the dimensionless frequency $\alpha_0 = L\alpha U_0^{-1}$. The second choice of U_0 corresponds to $\mathrm{Re}_\nu = 1$.

3. Invariant scaling, time averages and length scales

The incompressible Navier-Stokes equations possess the following well-known and powerful invariant scaling property involving an arbitrary parameter ℓ:

$$\boldsymbol{x}' = \ell^{-1}x; \quad t' = \ell^{-2}t; \quad \boldsymbol{u} = \ell^{-1}\boldsymbol{u}'; \tag{3.1}$$

which means that these equations are valid at every scale. The effect of this invariance is to scale the norms $\|\nabla^n\boldsymbol{u}\|_{2m}$ defined by

$$\|\nabla^n\boldsymbol{u}\|_{2m} = \left(\int_{V_d}|\nabla^n\boldsymbol{u}|^{2m}dV_d\right)^{1/2m} \tag{3.2}$$

in the following way:

$$\|\nabla^n\boldsymbol{u}\|_{2m} = \ell^{-1/\alpha_{m,n,d}}\|\nabla'^n\boldsymbol{u}'\|_{2m}\,, \tag{3.3}$$

where $\alpha_{n,m,d}$ is defined by[1]

$$\alpha_{n,m,d} = \frac{2m}{2m(n+1)-d}\,. \tag{3.4}$$

It is, therefore, clear that the $\alpha_{n,m,d}$ are a product of the invariance property (3.1). A dimensionless version of the norms defined in (3.3) is given by

$$F_{n,m,d} = \nu^{-1}L^{1/\alpha_{n,m,d}}\|\nabla^n\boldsymbol{u}\|_{2m}\,. \tag{3.5}$$

[1]The labelling of the dimensionless frequency α_0 and the exponents $\alpha_{n,m}$ is unfortunate, and could cause confusion, but we continue to use it to avoid the greater confusion of changing the notation from previous papers.

It has been shown that, for $d = 2, 3$, and for $n \geq 1$ and $1 \leq m \leq \infty$, weak solutions of the incompressible Navier-Stokes equations obey [29, 30]

$$\left\langle F_{n,m,d}^{(4-d)\alpha_{n,m,d}} \right\rangle_T \leq c_{n,m,d}\mathrm{Re}^3 \,. \tag{3.6}$$

The angular brackets $\langle \cdot \rangle_T$ represent the time average up to a time T, i.e.,

$$\langle \cdot \rangle_T = \frac{1}{T}\int_0^T \cdot \, d\tau \,. \tag{3.7}$$

We emphasize that these brackets represent a *time average*, not a statistical average. When $n = 0$ then m is restricted by $3 < m \leq \infty$. An example familiar to the reader is the case $n = m = 1$, in which case $(4 - d)\alpha_{1,1,d} = 2$ with the cancellation of the factor of $4 - d$. Then (3.6) yields the[2] familiar bound on the time-averaged energy dissipation rate

$$\varepsilon = \nu L^{-d} \left\langle \int_V |\boldsymbol{\omega}|^2 dV_d \right\rangle_T \leq \nu^3 L^{-4} \mathrm{Re}^3. \tag{3.8}$$

With the inverse Kolmogorov length defined by $\lambda_k^{-4} = \varepsilon/\nu^3$, we obtain the conventional bound

$$L\lambda_k^{-1} \leq \mathrm{Re}^{3/4} \,. \tag{3.9}$$

Equation (3.6) thus expresses an infinite hierarchy of such bounds and can be looked upon as weighted space-time averages of all derivatives of the velocity field in every L^{2m}-norm. There is an informal analogy with the concept of wavelets : higher derivatives reflect the dynamics at small scales, while increasing the value of m magnifies the larger amplitudes at each specific scale.

In [29, 30] it has also been shown how to define a set of inverse length scales associated with (3.6). Consider the set of t-dependent length-scales $\{\ell_{n,m,d}(t)\}$ defined by

$$\left(L\ell_{n,m,d}^{-1}\right)^{n+1} = F_{n,m,d} \,. \tag{3.10}$$

This definition takes into account the scaling of the domain volume L which makes (3.10) at the level of $n = m = 1$ and $d = 3$ consistent with the correct definition of the energy dissipation rate used to define the Kolmogorov length. Then we easily find that for Navier-Stokes weak solutions, when $n \geq 1$ and $1 \leq m \leq \infty$,

$$\left\langle L\ell_{n,m,d}^{-1} \right\rangle_T \leq c_{n,m,d} Re^{\frac{3}{(4-d)(n+1)\alpha_{n,m,d}}} \,. \tag{3.11}$$

When $d = 3$ and $n = m = 1$, then the exponent is $\frac{3}{4}$, as it should be. Also, note that $(n+1)\alpha_{n,m,d} \to 1$ as $n,\, m \to \infty$.

Of course, it has been known for many years that solutions of the two-dimensional Navier-Stokes equations are regular [26, 27], but expressing (3.6) in integer dimensions $d = 1, 2, 3$ rolls together into one line all the known two- and three-dimensional Navier-Stokes solution results, such as the class of weak solution $d = 3$ time averages found by Foias, Guillopé and Temam [28] in their pioneering paper in 1981. It has been explained in Ref. [29] that, for a full existence

[2]The vorticity $\boldsymbol{\omega}$ and the velocity gradient tensor $\nabla \boldsymbol{u}$ are synonymous in L^2 when $\mathrm{div}\, \boldsymbol{u} = 0$ but not in L^p for $p > 2$.

and uniqueness proof in the $d = 3$ case, a factor of $2\alpha_{n,m,3}$ would be needed as the exponent in (3.6). However, no evidence exists for the existence of bounds with this necessary factor of 2. It is possible that the Leray-Hopf weak solutions are all that exist.

By inspection it is clear that the ITT equations respect the invariant scaling possessed by the Navier-Stokes equations, apart from the linear-pumping term. However, there is a significant literature on a more general class of equations where the $\boldsymbol{u}|\boldsymbol{u}|^2$-term is replaced by $\boldsymbol{u}|\boldsymbol{u}|^{2\delta}$, which is the case in the Brinkman-Forchheimer extended Darcy model arising in porous media. The paper by Titi and Trabelsi [33] contains a wide literature survey; but we also refer the reader to [32, 34–44]. When $\delta > 1$, the invariant scaling property of the Navier-Stokes equations is broken. This leads to the bounding of time-averaged norms, higher than those available to ITT, which eventually lead to the regularity of solutions in the $d = 3$ case. The work in our paper is different in two important respects. Firstly, we use with the critical value $\delta = 1$ and thus remain faithful to the scaling property in (3.1). Secondly, the ITT equations in (2.4) have a linear term $\alpha_0\boldsymbol{u}$ which, while trivial in a purely functional setting, is nevertheless physically important in the creation of equilibrated or frozen states, which appear to dominate the dynamics in our DNSs.

The parallel scaling properties of the ITT equations and the Navier-Stokes equations suggest that the exponents $\alpha_{n,m,d}$ in (3.4) should be the same in both cases. Therefore, taking into account the factor of $4 - d$ in the exponent, we define

$$P_{n,m} = \|\nabla^n \boldsymbol{u}\|_{2m}^{2\alpha_{n,m,2}}\,, \qquad d = 2\,, \tag{3.12}$$

where

$$\alpha_{n,m,2} = \frac{m}{m(n+1)-1} \tag{3.13}$$

and a set of inverse length scales equivalent to (3.11)

$$\left\langle L\ell_{n,m,2}^{-1}\right\rangle_T \leq c_{n,m,2}\left\langle P_{n,m}\right\rangle_T^{\frac{1}{2(n+1)\alpha_{n,m,2}}}\,. \tag{3.14}$$

When $d = 3$

$$Q_{n,m} = \|\nabla^n \boldsymbol{u}\|_{2m}^{\alpha_{n,m,3}}\,, \qquad d = 3\,, \tag{3.15}$$

where

$$\alpha_{n,m,3} = \frac{2m}{2m(n+1)-3} \tag{3.16}$$

and a set of inverse length scales equivalent to (3.11)

$$\left\langle L\ell_{n,m,3}^{-1}\right\rangle_T \leq c_{n,m,3}\left\langle Q_{n,m}\right\rangle_T^{\frac{1}{(n+1)\alpha_{n,m,3}}}\,. \tag{3.17}$$

General bounds on $\langle P_{n,m}\rangle_T$, expressed as a function of α_0, Re_ν and $\mathscr{A}_0$, are expressed in §6. For $d = 3$, a narrower class of bounds on $\langle Q_{n,m}\rangle_T$ has been given in §7.

4. Energy estimates

In keeping with standard Navier-Stokes notation, we define n derivatives of $\boldsymbol{u}$ in $L^2(V_d)$ as

$$H_n = \int_{V_d} |\nabla^n \boldsymbol{u}|^2 dV_d\,. \tag{4.1}$$

Given the close relationship between the ITT equations and the incompressible Navier-Stokes equations, a formal approach is taken on the understanding that the standard Leray-Hopf weak-solution machinery, derived for the Navier-Stokes equations, is already in place [32, 33]. In this notation the energy H_0 and and enstrophy H_1 are:

$$\begin{aligned} H_0 &= \int_{V_d} |\boldsymbol{u}|^2 dV_d\,; && (4.2)\\ H_1 &= \int_{V_d} |\nabla\boldsymbol{u}|^2 dV_d = \int_{V_d} |\omega|^2 dV_d\,. && (4.3) \end{aligned}$$

A Leray-type energy inequality is easily derived

$$\tfrac{1}{2}\dot{H}_0 + \mathrm{Re}_\nu^{-1} H_1 + \mathrm{Re}_\beta \int_V |\boldsymbol{u}|^4 dV_d \leq \alpha_0 H_0 \tag{4.4}$$

from which we drop the H_1-term[3] and apply a Hölder inequality to the $\int_V |\boldsymbol{u}|^4 dV_d$-term to produce a simple differential inequality for H_0

$$\tfrac{1}{2}\dot{H}_0 \leq \alpha_0 H_0 - \mathrm{Re}_\beta H_0^2\,. \tag{4.5}$$

Thus, equilibration of the right hand side occurs at

$$H_{0,\,equil} = \alpha_0 \mathrm{Re}_\beta^{-1} \;\equiv\; \mathcal{A}_0\,, \tag{4.6}$$

where we designate $\mathcal{A}_0$ as the activity parameter. By using the time-average definition in (3.7), from (4.4) we find

$$\begin{aligned} \langle H_0\rangle_T &\leq \mathcal{A}_0\,, && (4.7)\\ \langle H_1\rangle_T &\leq \alpha_0\mathcal{A}_0\mathrm{Re}_\nu\,, && (4.8) \end{aligned}$$

together with the average of the L^4-norm

$$\left\langle \int_V |\boldsymbol{u}|^4 dV_d \right\rangle_T \leq \mathcal{A}_0^2\,. \tag{4.9}$$

The inequalities (4.7)–(4.9) each have an $O\left(T^{-1}\right)$ correction term that will be dropped from now on. These results are true in every dimension. At the level of H_0 the following 3 phenomena are possible :

1. For initial data $H_0(0) > \mathcal{A}_0$, we have control over H_0 because $\dot{H}_0 < 0$ in this region and H_0 decreases down to $\mathcal{A}_0$.
2. For initial data $H_0(0) < \mathcal{A}_0$, we find that $\dot{H}_0 \leq$ a +ve number. $\dot{H}_0(t)$ could be positive and thus H_0 will grow to reach $\mathcal{A}_0$ (a frozen state) but cannot pass through it.
3. For initial data $H_0(0) < \mathcal{A}_0$, despite the fact that $\dot{H}_0 \leq$ a +ve number, $\dot{H}_0$ could be negative, in which case H_0 decays.

The choice of $n = m = 1$ makes $(4-d)\alpha_{1,1,d} = 2$, whereupon the factor of $4-d$ cancels. Thus, from (4.8)

$$\left\langle P_{1,1}\right\rangle_T \leq \alpha_0\mathcal{A}_0\mathrm{Re}_\nu \tag{4.10}$$

and

$$\left\langle Q_{1,1}\right\rangle_T \leq \alpha_0\mathcal{A}_0\mathrm{Re}_\nu\,. \tag{4.11}$$

[3]Poincaré's inequality cannot be applied because, unlike the Navier-Stokes equations, the spatial average of $\boldsymbol{u}$ is not zero.

5. Numerical Methods

Run	d	N	δt	ν	α	β
A1	2	2048	2×10^{-4}	2.87×10^{-1}	10×10^{1}	5
A2	2	2048	2×10^{-4}	1.41×10^{-1}	10×10^{1}	5
A3	2	2048	2×10^{-4}	7.07×10^{-2}	10×10^{1}	5
A4	2	2048	2×10^{-4}	3.53×10^{-2}	10×10^{1}	5
A5	2	2048	2×10^{-4}	2.36×10^{-2}	10×10^{1}	5
A6	2	2048	2×10^{-4}	1.77×10^{-2}	10×10^{1}	5
A7	2	2048	2×10^{-4}	1×10^{-2}	10×10^{1}	5
A8	2	2048	2×10^{-4}	8.8×10^{-2}	10×10^{1}	5
B1	3	512	1×10^{-3}	5×10^{-1}	1×10^{1}	1×10^{-1}
B2	3	512	1×10^{-3}	5×10^{-2}	1×10^{1}	1×10^{-1}
B3	3	512	5×10^{-4}	1×10^{-2}	1×10^{1}	1×10^{-1}

Table 1: The parameters for our DNSs: d is the dimension, N^d the number of collocation points, and δ the time step.For all our runs, $\lambda = 1$. Given these parameters, the Reynolds numbers follow from Eqs. (2.2) and (2.5). Parameters for other runs are given in the Supplemental Material.

For our DNS of the d-dimensional ITT Eq. (2.1), we use a Fourier pseudospectral method [51] on periodic domains (a square in $d = 2$ and a cube in $d = 3$), with sides of length $L = 2\pi$, and N^d collocation points. We employ the second-order exponential time-difference scheme, ETDRK2, for time evolution in Fourier-space [52]. We list the parameters for our DNS runs in Table 1; parameters for additional DNS runs are given in the Supplemental Material.

The dimensional version of the ITT equations (2.1) has four parameters λ, α, ν and β which reduce to the three dimensionless numbers Re_ν, Re_β and α_0 in the non-dimensionalized version (2.4). As explained in (2.2), we have found it convenient to define the typical velocity field U_0 in two particular ways : $U_0 = \sqrt{\alpha/\beta}$ and $U_0 = \nu/L$. The latter case restricts Re_ν to the value $Re_\nu = 1$ but allows us to explore a more diverse range of α_0 and Re_β.

6. Summary of results in the $d = 2$ case

The methods used in the analysis sections of this paper are based on the differential inequalities explained in Appendix A. The proof of the results in the following subsections are given in Appendix B. Within these estimates, various multiplicative constants c, c_m and $c_{n,m}$ appear, which should be read as generic constants that may differ from line to line. These constants are algebraic in n, m but are not usually given explicitly : see Appendix A. We remark, furthermore, that while none of the bounds displayed in the following sections are saturated, this does not mean they are not sharp; more drastic initial conditions might get closer to saturation.

6.1. Estimates for $\langle P_{n,m}\rangle_T$

By using the definition of $P_{n,m}$ in (3.12) as our guide, for $m = 1$, we have $\alpha_{n,1,2} = 1/n$, so

$$\langle P_{n,1}\rangle_T = \left\langle H_n^{1/n}\right\rangle_T \, . \tag{6.1}$$

The estimate for $\langle P_{1,1}\rangle_T$ in (4.10) can be used to compute a series of other inequalities. The proofs can be found in Appendix B. Below is a summary :

(i) Firstly we wish to estimate $\langle P_{n,1}\rangle_T$ for $n \geq 1$. In inequality (B.7) in Appendix B.1, for $n = 2$ it is shown that

$$\langle P_{2,1}\rangle_T \leq c\,\alpha_0 \left(\alpha_0 \mathcal{A}_0 \mathrm{Re}_\nu^3\right)^{1/2} . \tag{6.2}$$

(ii) More generally, in inequality (B.22) Appendix B.5, it is shown that for $n \geq 2$

$$\langle P_{n,1}\rangle_T \quad \leq \quad c_{n,1}\alpha_0^{\frac{2}{n}} \left(\alpha_0 \mathcal{A}_0 \mathrm{Re}_\nu^3\right)^{\frac{n-1}{n}} . \tag{6.3}$$

(iii) In inequality (B.9) in Appendix B.2 it is shown that

$$\langle P_{1,m}\rangle_T = \left\langle \|\nabla \boldsymbol{u}\|_{2m}^{\frac{2m}{2m-1}} \right\rangle_T , \tag{6.4}$$

displayed in row 3 of Fig. 1, satisfies

$$\langle P_{1,m}\rangle_T \quad \leq \quad c_m \left(\alpha_0 \mathcal{A}_0 \mathrm{Re}_\nu\right)^{\frac{3m-2}{2m-1}} . \tag{6.5}$$

(iv) With the definition

$$\langle P_{0,m}\rangle_T = \left\langle \|\boldsymbol{u}\|_{2m}^{\frac{2m}{m-1}} \right\rangle_T , \tag{6.6}$$

from (B.13) in Appendix B.3, it is shown that, for $m > 2$,

$$\langle P_{0,m}\rangle_T \leq c\, \mathcal{A}_0^{\frac{m}{m-1}} \left(\alpha_0 \mathrm{Re}_\nu\right)^{\frac{m-2}{m-1}} . \tag{6.7}$$

(B.14) shows that, in the limit $m \to \infty$, we have

$$\langle P_{0,\infty}\rangle_T = \left\langle \|\boldsymbol{u}\|_\infty^2 \right\rangle_T \leq c\,\alpha_0 \mathcal{A}_0 \mathrm{Re}_\nu . \tag{6.8}$$

(v) In inequality (B.29) in Appendix B.6 it is shown that, for $n \geq 2$,

$$\langle P_{n,m}\rangle_T \leq c_{n,m}\alpha_0^{\frac{2m}{m(n+1)-1}} \left(\alpha_0 \mathcal{A}_0 \mathrm{Re}_\nu^3\right)^{\frac{mn-1}{m(n+1)-1}} . \tag{6.9}$$

(iv) Finally, in Appendix B.4 it is shown that global boundedness for the $2d$ ITT equations is also shown to exist in §Appendix B.4, by proving that H_1 is bounded point-wise in time for every $t > 0$.

6.2. *Numerical results for $P_{n,m}$*

We now present plots in Fig. 1 of $P_{n,m}(t)$ versus time t for the two values $n = 0$ and $n = 1$, with a sequence of values of $m = 1, \ldots, 10$. Hölder's inequality insists that, for fixed n, the norms $\|\cdot\|_{2m}$ must be ordered with increasing m, such that $\|\cdot\|_{2m} \leq \|\cdot\|_{2(m+1)}$; but the $\alpha_{n,m,d=2}$ *decrease* as m increases. Thus, it is technically possible for the $P_{n,m}$ to be ordered either way: i.e., an increasing regime $P_{n,m} \leq P_{n,m+1}$ or a decreasing regime $P_{n,m} \geq P_{n,m+1}$. The latter regime was originally observed numerically for the $d = 3$ NSEs [45, 46] and was also discussed in [47], although no obvious reason for this particular ordering was deduced. Moreover, no crossing of curves that represented different values of m was observed.

In all our runs for the $d = 2$ case, when $U_0 = \sqrt{\alpha/\beta}$ (panel A), we observe both regimes, but only the decreasing regime $P_{n,m} \geq P_{n,m+1}$ when $U_0 = \nu/L$ (panel B). We illustrate this with plots in Fig. 1 for run A6: In panel A ($U_0 = \sqrt{\alpha/\beta}$) the plots of $P_{1,m}$ can cross each other at different

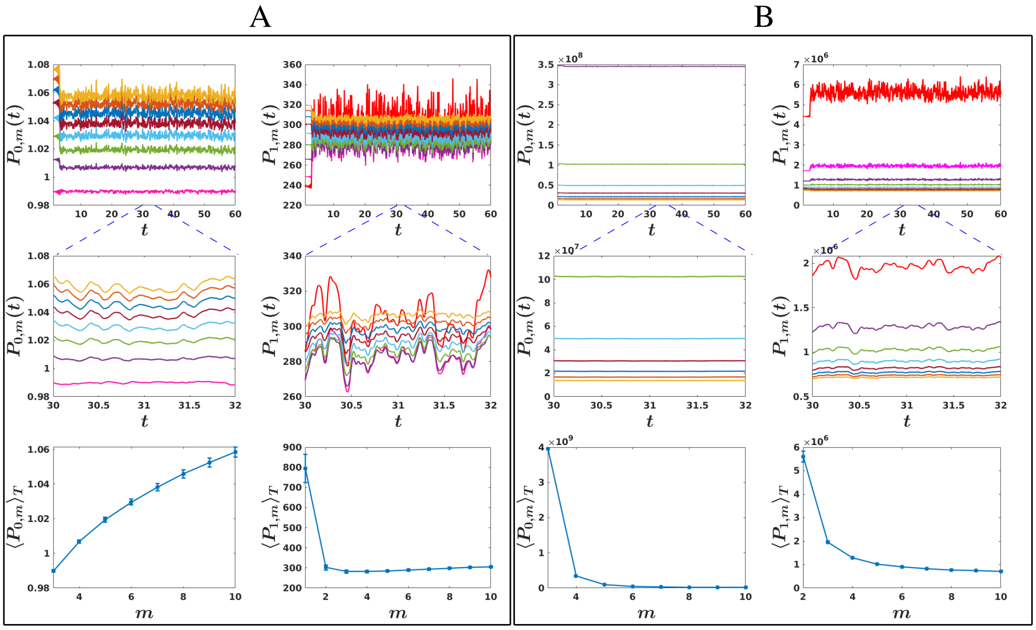

Figure 1: (colour online) Illustrative plots for $U_0 = \sqrt{\alpha/\beta}$ (panel A) and $U_0 = \nu/L$ (panel B) for run A6 (see Table 1): First and second rows: plots versus t of $P_{0,m}$ and $P_{1,m}$; the plots in the second row are expanded versions of small segments of the plots in the first row. Third row: Plots versus m of $\langle P_{0,m}\rangle_T$ and $\langle P_{1,m}\rangle_T$. Curves for $m = 2, 3, 4, 5, 6, 7, 8, 9,$ and 10 are drawn in red, pink; violet, green, cyan, maroon, blue, orange, and yellow, respectively. Similar plots for other representative runs are given in the Supplemental Material.

times, as we can see clearly in the expanded plots in the second rows; such crossings do not occur in panel B ($U_0 = \nu/L$). Furthermore, the plots versus m of $\langle P_{1,m}\rangle_T$ (third row) decreases monotonically with increasing m in panel B but not in panel A.

In Fig. 2 we give plots for $U_0 = \sqrt{\alpha/\beta}$ (panel A) and $U_0 = \nu/L$ (panel B), runs A1-A8, to illustrate whether the bound in 4.10 is saturated: In the first row we plot $\langle P_{1,1}\rangle_T$ (solid black line) versus Re_ν (panel A) and α_0 (panel B); the black dashed line denotes $Re_\nu\,\alpha_0\,\mathcal{A}_0$, which is the right-hand side (RHS) of (4.10) . In the second row we present plots versus Re_ν (panel A) and α_0 (panel B) of $\langle P_{0,m}\rangle_T$ and $\langle P_{1,m}\rangle_T$, for $m = 2, \ldots, 10$. Note that curves for $\langle P_{1,m}\rangle_T$ can cross as Re_ν increases (panel A); by contrast, they do not cross as α_0 increases (panel B). Similar plots for other representative runs are given in the Supplemental Material.

7. Summary of results in the $d = 3$ case

The proof of the results in the following subsections are given in Appendix C. The methods used there are based on the differential inequalities explained in Appendix A.

7.1. *Estimates for* $\langle Q_{n,m}\rangle_T$

Results in the $d = 3$ case are more restricted, which reflects the open status of the regularity problem. Nevertheless, time averages of various $Q_{n,m}$ of Navier-Stokes type can be found [29,

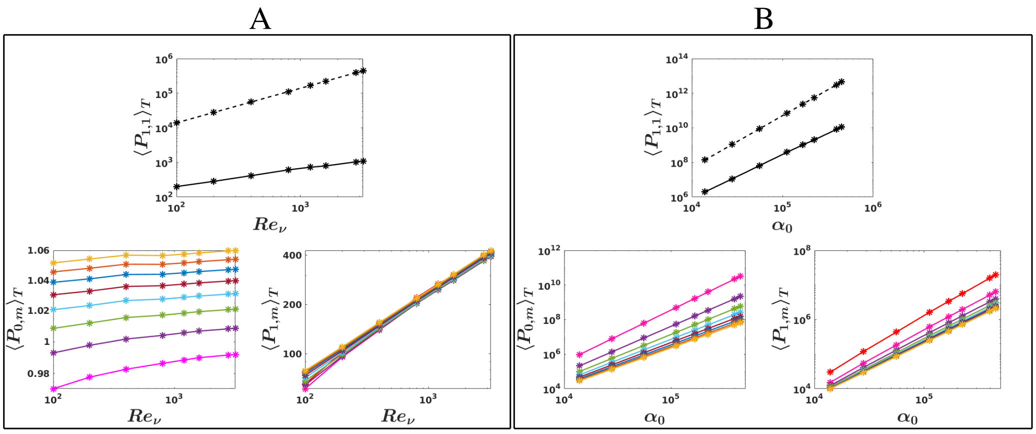

Figure 2: (Colour online) Illustrative plots for $U_0 = \sqrt{\alpha/\beta}$ (panel A) and $U_0 = \nu/L$ (panel B) for $d = 2$, runs A1-A8 (see Table 1): First row: plots versus Re_ν (panel A) and α_0 (panel B) of $\langle P_{1,1}\rangle_T$ (solid black line) and $Re_\nu\,\alpha_0\,\mathcal{A}_0$ (dashed black line). Second row: Plots versus Re_ν (panel A) and α_0 (panel B) of $\langle P_{0,m}\rangle_T$ and $\langle P_{1,m}\rangle_T$. Curves for $m = 2, 3, 4, 5, 6, 7, 8, 9$, and 10 are drawn in red, pink; violet, green, cyan, maroon, blue, orange, and yellow, respectively. Similar plots for other representative runs are given in the Supplemental Material.

30]. In addition to a bound on $\langle Q_{1,1}\rangle_T$, as in (4.11), our results from Appendix C are summarised thus: from (C.16) we have

$$\langle Q_{2,1}\rangle_T \le c\,\alpha_0 \mathrm{Re}_\nu^2. \tag{7.1}$$

We also find that for $n \ge 2$ and $m \ge 1$,

$$\langle Q_{n,m}\rangle_T < \infty \tag{7.2}$$

although estimating the right hand side is a difficult calculation that we have omitted (see (C.23)). Moreover, with

$$Q_{0,m} = \|\boldsymbol{u}\|_{2m}^{\frac{2m}{2m-3}}\,, \tag{7.3}$$

for $m > 2$, (7.4) shows that

$$\langle Q_{0,m}\rangle_T \le c\,\mathcal{A}_0^{\frac{2(m+3)}{5(2m-3)}}\left(\alpha_0 \mathrm{Re}_\nu^2\right)^{\frac{9(m-2)}{5(2m-3)}}\,. \tag{7.4}$$

(C.29) also shows that, in the limit $m \to \infty$,

$$\langle \|\boldsymbol{u}\|_\infty\rangle_T \quad\le\quad c\,\alpha_0^{9/10}\mathcal{A}_0^{1/5}\mathrm{Re}_\nu^{9/5}\,. \tag{7.5}$$

7.2. Numerical results for $Q_{n,m}$

Figure. 3 shows plots of $Q_{n,m}(t)$ versus time t for the two values $n = 0$ and $n = 1$, with a sequence of values of $m = 1, \ldots, 10$. Again, as in the $d = 2$ case, there are two regimes, namely, an increasing regime $Q_{n,m} \le Q_{n,m+1}$ and a decreasing regime $Q_{n,m} \ge Q_{n,m+1}$, because the norms $\|\cdot\|_{2m}$ must be ordered with increasing m, such that $\|\cdot\|_{2m} \le \|\cdot\|_{2(m+1)}$; but the $\alpha_{n,m,d=3}$ *decrease* as m increases.

In all our runs, when $U_0 = \sqrt{\alpha/\beta}$ (panel A) we observe both these regimes, but only the decreasing regime $Q_{n,m} \ge Q_{n,m+1}$ when $U_0 = \nu/L$ (panel B) has been used. We illustrate this

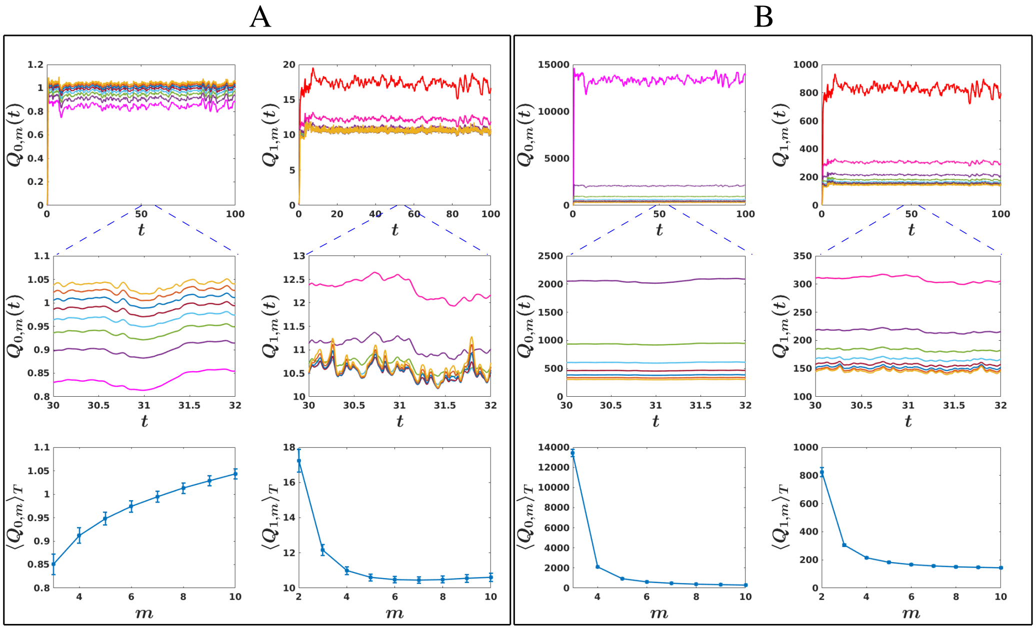

Figure 3: (Colour online) Illustrative plots for $U_0 = \sqrt{\alpha/\beta}$ (panel A) and $U_0 = \nu/L$ (panel B) for $d = 3$, run B2 (see Table 1): First and second rows: plots versus t of $Q_{0,m}$ and $Q_{1,m}$; the plots in the second row are expanded versions of small segments of the plots in the first row. Third row: Plots versus m of $\langle Q_{0,m}\rangle_T$ and $\langle Q_{1,m}\rangle_T$. Curves for $m = 2, 3, 4, 5, 6, 7, 8, 9$, and 10 are drawn in red, pink; violet, green, cyan, maroon, blue, orange, and yellow, respectively. Similar plots for other representative runs are given in the Supplemental Material.

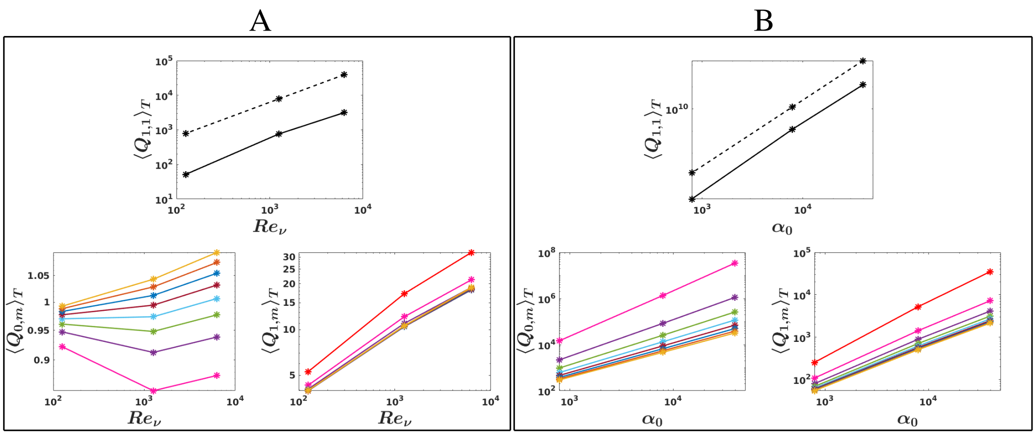

Figure 4: (Colour online) Illustrative plots for $U_0 = \sqrt{\alpha/\beta}$ (panel A) and $U_0 = \nu/L$ (panel B) for $d = 3$, runs A1-A8 (see Table 1): First row : plots versus Re_ν (panel A) and α_0 (panel B) of $\langle Q_{1,1}\rangle_T$ (solid black line) and $Re_\nu \alpha_0 \mathcal{A}_0$ (dashed black line). Second row : Plots versus Re_ν (panel A) and α_0 (panel B) of $\langle Q_{0,m}\rangle_T$ and $\langle Q_{1,m}\rangle_T$. Curves for $m = 1, 2, 3, 4, 5, 6, 7, 8, 9$, and 10 are drawn in black, red, pink, violet, green, cyan, maroon, blue, orange, and yellow, respectively. Similar plots for other representative runs are given in the Supplemental Material.

with plots in Fig. 3 for run B2 : In panel A ($U_0 = \sqrt{\alpha/\beta}$) the plots of $Q_{1,m}$ can cross each other at different times, as we can see clearly in the expanded plots in the second row; such crossings do not occur in panel B ($U_0 = \nu/L$). Furthermore, the plots versus m of $\langle Q_{1,m}\rangle_T$ (third row) decreases monotonically with increasing m in panel B but not in panel A. Note, in particular, that $Q_{1,m}$ is almost equivalent to a non-dimensionalized version of the $D_m = \|\omega\|_{2m}^{\alpha_{n,m,d=3}}$ introduced in [45] and plotted there for the $d = 3$ Navier-Stokes equations (see the Supplemental Material). The only difference here is that we are plotting $\|\nabla \boldsymbol{u}\|_{2m}$ and not $\|\boldsymbol{\omega}\|_{2m}$: the two are identical only when $m = 1$.

In Fig. 4 we present plots for $U_0 = \sqrt{\alpha/\beta}$ (panel A) and $U_0 = \nu/L$ (panel B), runs B1-B3, to illustrate whether the bound in (4.10) is saturated : In the first row we plot $\langle Q_{1,1}\rangle_T$ (panel B) ; the black dashed line denotes $Re_\nu\, \alpha_0\, \mathcal{A}_0$, which is the RHS of (4.10). In the second row we present plots versus Re_ν (panel A) and α_0 (panel B) of $\langle Q_{0,m}\rangle_T$ and $\langle Q_{1,m}\rangle_T$, for $m = 2, \ldots, 10$. Note that curves for $\langle Q_{1,m}\rangle_T$ can cross as Re_ν increases (panel A) ; by contrast, they do not cross as α_0 increases (panel B). Similar plots for other representative runs are given in the Supplemental Material.

8. Conclusions

In this paper we have married the two approaches of the analysis of weak solutions of the ITT equations, through the estimation of weighted time averages, together with the results of numerical simulations. To achieve this we have invoked the similar scaling properties between the ITT equations and the Navier-Stokes equations : see §3. There are, however, two important differences. Usually the Navier-Stokes equations are considered either in the decaying or the additively forced case, whereas the ITT equations have no additive forcing but instead have a linear-activity term $\alpha_0\boldsymbol{u}$ which, in effect, pumps energy into the system. This makes little difference to the functional nature of the problem, but dynamically the effect of this term, together with the negative cubic term, creates a platform for either temporally frozen solutions or statistically steady states. Furthermore, the greatest contrast with the $d = 2$ Navier-Stokes equations lies at the level of the vorticity equation. It can be easily shown that solutions of the forced $d = 2$ Navier-Stokes equations are regular. Indeed, the system has a global attractor whose dimension can be estimated : see references in [27]. The root cause of this is the absence of the vortex stretching term $\boldsymbol{\omega}\cdot\nabla\boldsymbol{u} = 0$, when $d = 2$, whereas, when $d = 3$, this term is not zero. The difference shows up at the level of the vorticity equation which can be expressed as

$$(\partial_t + \boldsymbol{u}\cdot\nabla)\,\boldsymbol{\omega} = (\alpha_0 + \mathrm{Re}_\nu)\,\Delta\boldsymbol{\omega} + \boldsymbol{\omega}\cdot\nabla\boldsymbol{u} - \mathrm{Re}_\beta\mathrm{curl}\left(\boldsymbol{u}|\boldsymbol{u}|^2\right).$$

For the ITT equations the $\mathrm{curl}\left(\boldsymbol{u}|\boldsymbol{u}|^2\right)$ term appears to destroy the regularity property held by the $d = 2$ Navier-Stokes equation, because it appears to be another form of vortex stretching. However, as we have shown above, the extra piece of information afforded to us is the bounded time integral expressed in (4.9)

$$\left\langle \int_V |\boldsymbol{u}|^4\, dV \right\rangle_T \leq \mathcal{A}_0^2\,, \tag{8.1}$$

which is enough to recover regularity, but only to the degree that bounds are exponential in time (see Appendix B.4). Thus, we fall just short of the Navier-Stokes result as we have no proof of the existence of a *global attractor*. Results that lie in parallel with those of the Navier-Stokes equations in both spatial dimensions is the existence of bounded infinite hierarchies of time averages : i.e., estimates of $\langle P_{n,m}\rangle_T$ and $\langle Q_{n,m}\rangle_T$, whose bounds are calculated in Appendix B and Appendix C and summarised in §6 and §7 together with the results of our numerical simulations.

When there are statistically steady solutions in our DNS, the possibility of multifractality should be considered [21, 22]. A future line of approach might be to repeat the calculation in [49], where the correspondence between the multifractal model of turbulence and the Navier–Stokes equations was investigated.

Acknowledgments : RP and JDG would like to thank the Isaac Newton Institute for Mathematical Sciences for support and hospitality during the programme *Mathematical Aspects of Fluid Turbulence : where do we stand?* in 2022, when work on this paper was undertaken. It was supported by grant number EP/R014604/1. RP, KVK and NBP thank SERB (India), the National Supercomputing Mission (India), and SERC (IISc), for support and computational resources, and A. Gupta for discussions.

Appendix A. Differential Inequalities

The most widely used class of differential inequalities that generalize the Sobolev inequalities are called Gagliardo-Nirenberg inequalities [50]. In their most general form in integer d dimensions ($d = 1, 2, 3$) they can be expressed as

$$\|\nabla^j u\|_p \leq c\,\|\nabla^n u\|_r^a \|u\|_q^{1-a}\,, \tag{A.1}$$

where $0 \leq j < n$ and $1 < p,\ r,\ q \leq \infty$. The exponent a can be calculated by dimensional analysis and thus must satisfy

$$\frac{1}{p} = \frac{j}{d} + a\left(\frac{1}{r} - \frac{n}{d}\right) + \frac{1-a}{q}\,, \tag{A.2}$$

where $j/m \leq a < 1$. (A.2) holds on the whole space $\mathbb{R}^d$. With periodic boundary conditions, there are L^2 additional terms, which produce lower-order corrections to our estimates, which will be ignored. In the following :

1. We take a formal approach on the understanding that the standard Leray-Hopf weak-solution machinery, derived for the Navier-Stokes equations, is already in place [32, 33].
2. We will use the convention that the constants designated as c, c_m or $c_{n,m}$ are generic in the sense that they may differ from line to line.

Appendix B. Proofs in the $d = 2$ case

Appendix B.1. Estimates for $\langle P_{2,1}\rangle_T$

Our first requirement is to bound $P_{2,1}$, with $P_{n,1}$ defined in (3.12). Clearly $\alpha_{n,1,2} = 1/n$, so

$$\begin{aligned}\langle P_{2,1}\rangle_T = \left\langle H_2^{1/2}\right\rangle_T &= \left\langle\left(\frac{H_2}{H_1}\right)^{1/2} H_1^{1/2}\right\rangle_T\\ &\leq \left\langle\frac{H_2}{H_1}\right\rangle_T^{1/2} \langle P_{1,1}\rangle_T^{1/2}\,.\end{aligned} \tag{B.1}$$

To achieve a bound on $\langle H_2/H_1\rangle_T$, we take the curl of the ITT equation :

$$(\partial_t + \boldsymbol{u}\cdot\nabla)\,\boldsymbol{\omega} = \alpha_0\boldsymbol{\omega} + \mathrm{Re}_\nu^{-1}\Delta\boldsymbol{\omega} - \mathrm{Re}_\beta\,\mathrm{curl}(\boldsymbol{u}|\boldsymbol{u}|^2)\,. \tag{B.2}$$

The key point is that, while the vortex-stretching term $\boldsymbol{\omega}\cdot\nabla\boldsymbol{u}$ is missing because of the orthogonality of $\boldsymbol{\omega}$ with the gradient operator, there is an additional negative $\mathrm{Re}_\beta\,\mathrm{curl}(\boldsymbol{u}|\boldsymbol{u}|^2)$-term. To deal with this we write

$$\begin{aligned}\tfrac{1}{2}\dot{H}_1 &\leq \alpha_0 H_1 - \mathrm{Re}_\nu^{-1}H_2 - \mathrm{Re}_\beta\int_V \boldsymbol{\omega}\cdot\mathrm{curl}(\boldsymbol{u}|\boldsymbol{u}|^2)dV\\ &\leq \alpha_0 H_1 - \tfrac{1}{2}\mathrm{Re}_\nu^{-1}H_2 + \tfrac{1}{2}\mathrm{Re}_\beta^2\mathrm{Re}_\nu\int_V|\boldsymbol{u}|^6 dV\,,\end{aligned} \tag{B.3}$$

where we have integrated by parts and have then used a Hölder inequality. Now divide by H_1 to obtain

$$\tfrac{1}{2}\left\langle\frac{H_2}{H_1}\right\rangle_T \leq \mathrm{Re}_\nu\alpha_0 + \tfrac{1}{2}\mathrm{Re}_\beta^2\mathrm{Re}_\nu^2\left\langle\frac{\int_V|\boldsymbol{u}|^6dV}{H_1}\right\rangle_T\,.$$

Then we use a Gagliardo-Nirenberg inequality

$$\|\boldsymbol{u}\|_6 \leq c\,\|\nabla\boldsymbol{u}\|_2^a\|\boldsymbol{u}\|_4^{1-a}\,,\qquad a=\tfrac{1}{3}\,, \tag{B.4}$$

to find

$$\left\langle\frac{\|\boldsymbol{u}\|_6^6}{H_1}\right\rangle_T \leq c\,\left\langle\|\boldsymbol{u}\|_4^4\right\rangle_T\,. \tag{B.5}$$

Inserting this into (B.4) gives

$$\begin{aligned}\tfrac{1}{2}\left\langle\frac{H_2}{H_1}\right\rangle_T &\leq \alpha_0\mathrm{Re}_\nu + c\,\mathrm{Re}_\beta^2\mathrm{Re}_\nu^2\left\langle\|\boldsymbol{u}\|_4^4\right\rangle_T\\ &\leq c\,\alpha_0\mathrm{Re}_\nu\,(1+\alpha_0\mathrm{Re}_\nu)\,.\end{aligned} \tag{B.6}$$

Thus, to leading order in Re_ν, (B.1) becomes

$$\langle P_{2,1}\rangle_T \lessapprox c\,\mathcal{A}_0^{1/2}\,(\alpha_0\mathrm{Re}_\nu)^{3/2}\,, \tag{B.7}$$

as advertised in (6.3).

Appendix B.2. An estimate for $P_{1,m} = \left\langle\|\nabla\boldsymbol{u}\|_{2m}^{\frac{2m}{2m-1}}\right\rangle_T$

A Gagliardo-Nirenberg inequality shows that, for some function A ,

$$\|A\|_{2m} \leq c_m\|\nabla A\|_2^{\frac{m-1}{m}}\,\|A\|_2^{\frac{1}{m}}\,. \tag{B.8}$$

We choose $A=\nabla\boldsymbol{u}$ and, noting from (3.4) that $\alpha_{1,m,2} = m/(2m-1)$, we write

$$\begin{aligned}\left\langle\|\nabla\boldsymbol{u}\|_{2m}^{\frac{2m}{2m-1}}\right\rangle_T &\leq c_m\left\langle\|\nabla^2\boldsymbol{u}\|_2^{\frac{2(m-1)}{2m-1}}\,\|\nabla\boldsymbol{u}\|_2^{\frac{2}{2m-1}}\right\rangle_T\\ &\leq c_m\left\langle\|\nabla^2\boldsymbol{u}\|_2\right\rangle_T^{\frac{2(m-1)}{2m-1}}\,\left\langle\|\nabla\boldsymbol{u}\|_2^2\right\rangle_T^{\frac{1}{2m-1}}\\ &= c_m\,\langle P_{2,1}\rangle_T^{\frac{2(m-1)}{2m-1}}\,\langle H_1\rangle_T^{\frac{1}{2m-1}}\\ &\leq c_m\,(\alpha_0\mathcal{A}_0\mathrm{Re}_\nu)^{\frac{3m-2}{2m-1}}\,,\end{aligned} \tag{B.9}$$

as advertised in (6.5). In the limit $m\to\infty$,

$$\langle\|\nabla\boldsymbol{u}\|_\infty\rangle_T \leq c\,(\alpha_0\mathcal{A}_0\mathrm{Re}_\nu)^{3/2}\,. \tag{B.10}$$

Appendix B.3. Estimates for $\langle P_{0,m}\rangle_T = \left\langle \|\boldsymbol{u}\|_{2m}^{\frac{2m}{m-1}}\right\rangle_T$ and $\left\langle \|\boldsymbol{u}\|_\infty^2\right\rangle_T$

We now turn to estimating $\boldsymbol{u}$ in $L^{2m}(V)$ for $m > 2$.

$$\|\boldsymbol{u}\|_{2m} \leq c_m \|\nabla^2\boldsymbol{u}\|_2^{\frac{m-2}{3m}} \|\boldsymbol{u}\|_4^{\frac{m-2}{3m}}\,, \tag{B.11}$$

where $a = \frac{m-2}{3m}$. When $n = 0$ and $d = 2$ we have $(4-d)\alpha_{0,m,2} = \frac{2m}{m-1}$. Thus,

$$\begin{aligned} \left\langle \|\boldsymbol{u}\|_{2m}^{\frac{2m}{m-1}}\right\rangle_T &\leq c_m \left\langle \|\nabla^2\boldsymbol{u}\|_2^{\frac{2(m-2)}{3(m-1)}} \|\boldsymbol{u}\|_4^{\frac{4(m+1)}{3(m-1)}}\right\rangle_T \\ &\leq \langle P_{2,1}\rangle_T^{\frac{2(m-2)}{3(m-1)}} \left\langle \|\boldsymbol{u}\|_4^4\right\rangle_T^{\frac{(m+1)}{3(m-1)}}\,, \end{aligned} \tag{B.12}$$

in which case, for $m > 2$, using (B.7) and (4.9),

$$\left\langle \|\boldsymbol{u}\|_{2m}^{\frac{2m}{m-1}}\right\rangle_T \leq c\,\mathcal{A}_0^{\frac{m}{(m-1)}} \left(\alpha_0 \mathrm{Re}_\nu\right)^{\frac{m-2}{m-1}}\,, \tag{B.13}$$

as advertised in (6.7). In the limit $m \to \infty$, this reduces to

$$\left\langle \|\boldsymbol{u}\|_\infty^2\right\rangle_T \leq c\,\alpha_0 \mathcal{A}_0 \mathrm{Re}_\nu\,, \tag{B.14}$$

as advertised in (6.8).

Appendix B.4. Regularity: an exponential bound in $d = 2$ dimensions

Returning to (B.5) we can write

$$\tfrac{1}{2}\dot{H}_1 \leq \left(\alpha_0 + \tfrac{1}{2}\mathrm{Re}_\beta^2 \mathrm{Re}_\nu \|\boldsymbol{u}\|_4^4\right) H_1 \tag{B.15}$$

and so

$$\begin{aligned} H_1(T) &\leq H_1(0)\exp\left\{\int_0^T \left(\alpha_0 + c\,\mathrm{Re}_\beta^2\mathrm{Re}_\nu\|\boldsymbol{u}\|_4^4\right) d\tau\right\} \\ &\leq H_1(0)\exp\left\{\alpha_0\left(1 + c\,\mathrm{Re}_\beta^2\mathrm{Re}_\nu\mathcal{A}_0^2\right) T\right\}\,, \end{aligned} \tag{B.16}$$

which is finite for every finite T. Control over the H_1-norm establishes global regularity in this $2d$ case but not a global attractor, which requires a uniform bound for all t.

Appendix B.5. Estimates for $\langle P_{n,1}\rangle_T$ for $n > 2$

Using the methods in [27], a full 'ladder' for H_n takes the form

$$\begin{aligned} \tfrac{1}{2}\dot{H}_n &\leq \alpha_0 H_n - \mathrm{Re}_\nu^{-1} H_{n+1} + c_{n,1} H_{n+1}^{1/2} H_n^{1/2} \|\boldsymbol{u}\|_\infty \\ &+ c_{n,2}\mathrm{Re}_\beta H_n \|\boldsymbol{u}\|_\infty^2\,; \end{aligned} \tag{B.17}$$

therefore, after a Hölder inequality and re-arrangement, we have

$$\tfrac{1}{2}\dot{H}_n \leq \alpha_0 H_n - \tfrac{1}{2}\mathrm{Re}_\nu^{-1} H_{n+1} + c_n\left(\mathrm{Re}_\beta + \mathrm{Re}_\nu\right) H_n \|\boldsymbol{u}\|_\infty^2\,. \tag{B.18}$$

Thus,

$$\left\langle \frac{H_{n+1}}{H_n}\right\rangle_T \leq 2\alpha_0 \mathrm{Re}_\nu + c_n \mathrm{Re}_\nu\left(\mathrm{Re}_\beta + \mathrm{Re}_\nu\right)\left\langle \|\boldsymbol{u}\|_\infty^2\right\rangle_T \tag{B.19}$$

from which we deduce that

$$\left\langle \frac{H_{n+1}}{H_n} \right\rangle_T \quad \lessapprox \quad c_n \alpha_0 \mathcal{A}_0 \mathrm{Re}_\nu^3 \,. \tag{B.20}$$

Moreover, for $n \geq 2$

$$\begin{aligned} \langle P_{n+1,1} \rangle_T &= \left\langle \left(\frac{H_{n+1}}{H_n} \right)^{\frac{1}{n+1}} H_n^{\frac{1}{n+1}} \right\rangle_T \\ &\leq \left\langle \frac{H_{n+1}}{H_n} \right\rangle_T^{\frac{1}{n+1}} \langle P_{n,1} \rangle_T^{\frac{n}{n+1}} \,. \end{aligned} \tag{B.21}$$

Given that $\langle P_{2,1} \rangle_T$ is bounded above as in (B.7), together with (B.20), we can now generate upper bounds on every $\langle P_{n,1} \rangle_T$ for $n \geq 2$, namely,

$$\langle P_{n,1} \rangle_T \quad \leq \quad c_{n,1} \alpha_0^{\frac{n+1}{n}} \mathcal{A}_0^{\frac{n-1}{n}} \mathrm{Re}_\nu^{\frac{3(n-1)}{n}} \,, \tag{B.22}$$

which can be transformed into the form advertised in (6.3).

Appendix B.6. Estimates for $\langle P_{n,m} \rangle_T$

We can write down an inequality for $B = \nabla^2 \boldsymbol{u}$ such that

$$\|\nabla^{n-2} B\|_{2m} \leq c\, \|\nabla^{N-2} B\|_2^a \|B\|_2^{1-a} \,, \tag{B.23}$$

for some $N > n + 1 - 1/m$, with

$$a = \frac{m(n-1) - 1}{m(n+1) - 1} \,. \tag{B.24}$$

Thus, we can write

$$\left\langle \|\nabla^n \boldsymbol{u}\|_{2m}^{2\alpha_{n,m}} \right\rangle_T \leq c \left\langle \|\nabla^N \boldsymbol{u}\|_2^{2a\alpha_{n,m}} \|\nabla^2 \boldsymbol{u}\|_2^{2(1-a)\alpha_{n,m}} \right\rangle_T \,. \tag{B.25}$$

Re-arranging and then using Hölder's inequality, we have

$$\left\langle \|\nabla^n \boldsymbol{u}\|_{2m}^{2\alpha_{n,m}} \right\rangle_T \quad \leq \quad c \left\langle \left(\|\nabla^N \boldsymbol{u}\|_2^{2/N} \right)^{aN\alpha_{n,m}} \left(\|\nabla^2 \boldsymbol{u}\|_2 \right)^{2(1-a)\alpha_{n,m}} \right\rangle_T \tag{B.26}$$

$$\leq \quad c_{N,n,m} \left\langle \|\nabla^N \boldsymbol{u}\|_2^{2/N} \right\rangle_T^{aN\alpha_{n,m}} \left\langle \|\nabla^2 \boldsymbol{u}\|_2^{\frac{2(1-a)\alpha_{n,m}}{1-aN\alpha_{n,m}}} \right\rangle_T^{1-aN\alpha_{n,m}} \tag{B.27}$$

$$= \quad c_{N,n,m} \langle P_{N,1} \rangle_T^{aN\alpha_{n,m}} \left\langle P_{2,1}^{\frac{2(1-a)\alpha_{n,m}}{1-aN\alpha_{n,m}}} \right\rangle_T^{1-aN\alpha_{n,m}} \,. \tag{B.28}$$

It can be checked through the definition of a in (B.24) that the exponent of $P_{2,1}$ inside the time-average is unity. Estimates for $\langle P_{N,1} \rangle_T$ and $\langle P_{2,1} \rangle_T$ are available from (6.3) and (6.2): one can then choose the lowest value of N, constrained by $N > n + 1 - 1/m$. After some algebra, this leads to the result

$$\langle P_{n,m} \rangle_T \leq c_{n,m} \alpha_0^{\frac{2m}{m(n+1)-1}} \left(\alpha_0 \mathcal{A}_0 \mathrm{Re}_\nu^3 \right)^{\frac{mn-1}{m(n+1)-1}} \,, \tag{B.29}$$

as advertised in (6.9).

Appendix C. Proofs in the $d = 3$ case

Step 1 : $Q_{n,m}$ is defined in (3.15). In simplied form $Q_{n,1}$ can be written as

$$Q_{n,1} = H_n^{\frac{1}{2n-1}} . \tag{C.1}$$

Moreover, because $\langle Q_{1,1}\rangle_T = \langle H_1\rangle_T$, we have an estimate for this in (4.8). We begin this section by estimating $\langle Q_{2,1}\rangle_T$ from the vorticity equation (B.2), with the $3d$ vortex stretching term restored:

$$(\partial_t + \boldsymbol{u}\cdot\nabla)\,\boldsymbol{\omega} = \alpha_0\boldsymbol{\omega} + \mathrm{Re}_\nu^{-1}\Delta\boldsymbol{\omega} + \boldsymbol{\omega}\cdot\nabla\boldsymbol{u} - \mathrm{Re}_\beta\,\mathrm{curl}(\boldsymbol{u}|\boldsymbol{u}|^2)\,. \tag{C.2}$$

From now on, all the steps are formal : all estimates are based on weak-solution theory. The equivalent of (B.3) is

$$\begin{aligned}\tfrac{1}{2}\dot{H}_1 &\leq \alpha_0 H_1 - \mathrm{Re}_\nu^{-1}H_2 + H_2^{1/2}H_1^{1/2}\|\boldsymbol{u}\|_\infty - \mathrm{Re}_\beta\int_V \boldsymbol{\omega}\cdot\mathrm{curl}(\boldsymbol{u}|\boldsymbol{u}|^2)dV\\ &\leq \alpha_0 H_1 - \tfrac{3}{4}\mathrm{Re}_\nu^{-1}H_2 + H_2^{1/2}H_1^{1/2}\|\boldsymbol{u}\|_\infty + \mathrm{Re}_\beta^2\mathrm{Re}_\nu\int_V |\boldsymbol{u}|^6 dV\,,\end{aligned} \tag{C.3}$$

where we have integrated by parts and have then used a Hölder inequality. The 3-dimensional Agmon inequality for $\|\boldsymbol{u}\|_\infty$ is

$$\|\boldsymbol{u}\|_\infty^2 \leq c_n H_n^a H_1^{1-a} \qquad n \geq 2\,, \tag{C.4}$$

with $a = \frac{1}{2(n-1)}$. Thus, for $n = 2$,

$$\|\boldsymbol{u}\|_\infty \leq c\, H_2^{1/4}H_1^{1/4} \tag{C.5}$$

and so

$$\begin{aligned}H_2^{1/2}H_1^{1/2}\|\boldsymbol{u}\|_\infty &\leq c\,H_2^{3/4}H_1^{3/4} &\text{(C.6)}\\ &\leq \tfrac{1}{4}\mathrm{Re}_\nu^{-1}H_2 + c\,\mathrm{Re}_\nu^3 H_1^3\,. &\text{(C.7)}\end{aligned}$$

Moreover, Sobolev's inequality for $d = 3$ shows that

$$\|\boldsymbol{u}\|_6 \leq c\,\|\nabla\boldsymbol{u}\|_2\,; \tag{C.8}$$

therefore, in total, (C.3) becomes

$$\tfrac{1}{2}\dot{H}_1 \leq \alpha_0 H_1 - \tfrac{1}{4}\mathrm{Re}_\nu^{-1}H_2 + c\,\mathrm{Re}_\nu\left(\mathrm{Re}_\beta^2 + \mathrm{Re}_\nu^2\right)H_1^3\,. \tag{C.9}$$

Thus, the ultimate contribution to (C.10) from the $\boldsymbol{u}|\boldsymbol{u}|^2$-term is proportional to that from the vortex-stretching term, in the sense that they are both proportional to H_1^3. Dividing by H_1^2 gives

$$\tfrac{1}{4}\mathrm{Re}_\nu^{-1}\left\langle\frac{H_2}{H_1^2}\right\rangle_T \leq \alpha_0\left\langle H_1^{-1}\right\rangle_T + c\,\mathrm{Re}_\nu\left(\mathrm{Re}_\beta^2 + \mathrm{Re}_\nu^2\right)Q_1\,. \tag{C.10}$$

Ignoring the first term on the right hand side with the negative exponent, we can write

$$\left\langle\frac{H_2}{H_1^2}\right\rangle_T \leq c\,\alpha_0\mathrm{Re}_\nu^2\left(\mathrm{Re}_\beta^2 + \mathrm{Re}_\nu^2\right)\,. \tag{C.11}$$

In this part we finally have

$$\begin{aligned}
\langle Q_{2,1}\rangle_T &= \left\langle\left(\frac{H_2}{H_1^2}\right)^{1/3} H_1^{2/3}\right\rangle_T && \text{(C.12)}\\
&\le \left\langle\frac{H_2}{H_1^2}\right\rangle_T^{1/3} \langle H_1\rangle_T^{2/3} && \text{(C.13)}\\
&\le c\left(\alpha_0 \mathrm{Re}_\nu^2\left(\mathrm{Re}_\beta^2+\mathrm{Re}_\nu^2\right)\right)^{1/3} (\alpha_0\mathrm{Re}_\nu)^{2/3} && \text{(C.14)}\\
&= c\,\alpha_0 \mathrm{Re}_\nu^{4/3}\left(\mathrm{Re}_\beta^2+\mathrm{Re}_\nu^2\right)^{1/3}\,. && \text{(C.15)}
\end{aligned}$$

Since Re_ν is dominant, the bound on Q_2 scales like

$$\langle Q_{2,1}\rangle_T \lessapprox \alpha_0\mathrm{Re}_\nu^2 + O\left(\mathrm{Re}_\nu^{4/3}\right)\,. \tag{C.16}$$

Step 2 : Let us repeat (B.18) by writing

$$\tfrac{1}{2}\dot{H}_n \le \alpha_0 H_n - \tfrac{1}{2}\mathrm{Re}_\nu^{-1}H_{n+1} + c_n\left(\mathrm{Re}_\beta+\mathrm{Re}_\nu\right)H_n\|\boldsymbol{u}\|_\infty^2\,. \tag{C.17}$$

After re-arrangement and the use of Agmon's inequality, (C.17) becomes

$$\tfrac{1}{2}\dot{H}_n \le \alpha_0 H_n - \tfrac{1}{2}\mathrm{Re}_\nu^{-1}H_{n+1} + c_n\left(\mathrm{Re}_\beta+\mathrm{Re}_\nu\right)H_n^{1+a}H_1^{1-a}\,. \tag{C.18}$$

Dividing by $H_n^{2n/(2n-1)}$ and time averaging gives

$$\begin{aligned}
\tfrac{1}{2}\mathrm{Re}_\nu^{-1}\left\langle\frac{H_{n+1}}{H_n^{\frac{2n}{2n-1}}}\right\rangle_T &\le \alpha_0\left\langle H_n^{1-\frac{2n}{2n-1}}\right\rangle_T + c_n\left(\mathrm{Re}_\beta+\mathrm{Re}_\nu\right)\left\langle H_n^{\frac{2n-1}{2(n-1)}-\frac{2n}{2n-1}} H_1^{\frac{2n-3}{2(n-1)}}\right\rangle_T \\
&\le \alpha_0\left\langle H_n^{-\frac{1}{2n-1}}\right\rangle_T + c_n\left(\mathrm{Re}_\beta+\mathrm{Re}_\nu\right)\langle Q_n\rangle_T^{\frac{1}{2(n-1)}}\langle Q_1\rangle^{\frac{2n-3}{2(n-1)}}\,. && \text{(C.19)}
\end{aligned}$$

The next step is to ignore the first term[4]. Given that Re_ν is the dominant term, we write (C.19) in the simplified form

$$\left\langle\frac{H_{n+1}}{H_n^{\frac{2n}{2n-1}}}\right\rangle_T \le c_n\mathrm{Re}_\nu^2\langle Q_{n,1}\rangle_T^{\frac{1}{2(n-1)}}\langle Q_{1,1}\rangle_T^{\frac{2n-3}{2(n-1)}}\,. \tag{C.20}$$

We then study

$$\begin{aligned}
\langle Q_{n+1,1}\rangle_T = \left\langle H_{n+1}^{\frac{1}{2n+1}}\right\rangle_T &= \left\langle\left(\frac{H_{n+1}}{H_n^{\frac{2n}{2n-1}}}\right)^{\frac{1}{2n+1}} H_n^{\frac{2n}{(2n+1)(2n-1)}}\right\rangle_T \\
&\le \left\langle\frac{H_{n+1}}{H_n^{\frac{2n}{2n-1}}}\right\rangle_T^{\frac{1}{2n+1}}\langle Q_{n,1}\rangle_T^{\frac{2n}{2n+1}}\,, && \text{(C.21)}
\end{aligned}$$

[4]The term with the negative exponent of H_n on the RHS of (C.19) is only out of control if H_n temporarily becomes very small. In principle, this could be dealt with by adding a constant term to H_n to provide the platform of a lower bound. We omit the details.

in which case

$$\begin{aligned}\langle Q_{n+1,1}\rangle_T &\le c_n \mathrm{Re}_\nu^{\frac{2}{2n+1}} \langle Q_{n,1}\rangle_T^{\frac{2n}{2n+1}+\frac{1}{2(2n+1)(n-1)}} \langle Q_{1,1}\rangle_T^{\frac{2n-3}{2(n-1)(2n+1)}}\\ &= c_n \mathrm{Re}_\nu^{\frac{2}{2n+1}} \langle Q_{n,1}\rangle_T^{\frac{(2n-1)^2}{2(2n+1)(n-1)}} \langle Q_{1,1}\rangle_T^{\frac{2n-3}{2(n-1)(2n+1)}}\,.\end{aligned} \tag{C.22}$$

Given that we have estimates for both $\langle Q_{1,1}\rangle_T$ and $\langle Q_{2,1}\rangle_T$, we can generate estimates for all $\langle Q_{n,1}\rangle_T$ for $n \ge 3$. Thus, we can write

$$\langle Q_{n,1}\rangle_T < \infty \qquad n \ge 3\,. \tag{C.23}$$

Then the method used in §Appendix B.6 can be used to show that $\langle Q_{n,m}\rangle_T < \infty$ for $m \ge 1$.

Step 3 : Now let us consider

$$\|\boldsymbol{u}\|_{2m} \le c\,\|\nabla^2\boldsymbol{u}\|_2^a\|\boldsymbol{u}\|_4^{1-a}\,, \tag{C.24}$$

where $a = 3(m-2)/5m$ with $m > 2$. Then we can write

$$\begin{aligned}\left\langle\|\boldsymbol{u}\|_{2m}^{\alpha_{0,m}}\right\rangle_T &\le c\left\langle\|\nabla^2\boldsymbol{u}\|_2^{a\alpha_{0,m}}\|\nabla\boldsymbol{u}\|_4^{(1-a)\alpha_{0,m}}\right\rangle_T\\ &= c\left\langle Q_{2,1}^{3a\alpha_{0,m}/2}\left(\|\boldsymbol{u}\|_4^4\right)^{\frac{1}{4}(1-a)\alpha_{0,m}/2}\right\rangle_T\,,\end{aligned} \tag{C.25}$$

where $\alpha_{0,m} = \frac{2m}{2m-3}$. Then

$$\left\langle\|\boldsymbol{u}\|_{2m}^{\alpha_{0,m}}\right\rangle_T \le c\,\langle Q_{2,1}\rangle_T^{3a\alpha_{0,m}/2}\left\langle\left(\|\boldsymbol{u}\|_4^4\right)^{\frac{\frac{1}{4}(1-a)\alpha_{0,m}/2}{1-3a\alpha_{0,m}/2}}\right\rangle_T^{1-3a\alpha_{0,m}/2}\,. \tag{C.26}$$

Given a and $\alpha_{0,m}$, it can easily be checked that the exponent of $\|\boldsymbol{u}\|_4^4$ inside the average is unity. Thus, because $\left\langle\|\boldsymbol{u}\|_4^4\right\rangle_T \le c\,\mathcal{A}_0^2$, (C.26) becomes

$$\begin{aligned}\left\langle\|\boldsymbol{u}\|_{2m}^{\alpha_{0,m}}\right\rangle_T &\le c\,(\alpha_0\mathrm{Re}_\nu^2)^{3a\alpha_{0,m}/2}\mathcal{A}_0^{2-3a\alpha_{0,m}}\\ &= \alpha_0^{3a\alpha_{0,m}/2}\mathcal{A}_0^{2-3a\alpha_{0,m}}\mathrm{Re}_\nu^{3a\alpha_{0,m}}\,.\end{aligned} \tag{C.27}$$

In fact $3a\alpha_{0,m}/2 = \frac{9(m-2)}{5(2m-3)}$ and so $1 - 3a\alpha_{0,m}/2 = \frac{m+3}{5(2m-3)}$, whence

$$\left\langle\|\boldsymbol{u}\|_{2m}^{\alpha_{0,m}}\right\rangle_T \le c\,\alpha_0^{\frac{9(m-2)}{5(2m-3)}}\mathcal{A}_0^{\frac{2(m+3)}{5(2m-3)}}\mathrm{Re}_\nu^{\frac{18(m-2)}{5(2m-3)}} \qquad m > 2\,, \tag{C.28}$$

as advertised in (7.4). In the limit $m \to \infty$, we find that

$$\langle\|\boldsymbol{u}\|_\infty\rangle_T \le c\,\alpha_0^{9/10}\mathcal{A}_0^{1/5}\mathrm{Re}_\nu^{9/5}\,, \tag{C.29}$$

as advertised in (7.5).

References

[1] C. W. Reynolds, in Proceedings of the 14th Annual Conference on Computer Graphics and Interactive Techniques, ACM Press, (1987) pp. 25–34.

[2] T. Vicsek, A. Czirok, E. Ben-Jacob, I. Cohen, and O. Shochet, Novel Type of Phase, Transition in a System of Self-Driven Particles, Phys. Rev. Lett. **75** (1995) 1226–1229.

[3] A. Czirok, H. E. Stanley, and T. Vicsek, Spontaneously ordered motion of self-propelled particles, J. Phys. A **30** (1997) 1375–1385.
[4] J. Toner and Y. Tu, Long-Range Order in a Two-Dimensional Dynamical XYModel: How Birds Fly Together, Phys. Rev. Lett. **75** (1995) 4326–4329.
[5] J. Toner, Y. Tu, and S. Ramaswamy, Hydrodynamics and phases of flocks, Ann. Phys. **318** (2005) 170–244.
[6] R. Alert, J.-F. Joanny, and J. Casademunt, Universal scaling of active nematic turbulence, Nature Physics **16** (2020) 682–688. doi.org/10.1038/s41567-020-0854-4 .
[7] H. H. Wensink, J. Dunkel, S. Heidenreich, K. Drescher, R. E. Goldstein, H. Löwen, and J. M. Yeomans, Meso-scale turbulence in living fluids, Proc. Nat. Acad. Sci. **109** (2012) 14308–13.
[8] J. Dunkel, S. Heidenreich, K. Drescher, H. H. Wensink, M. Bär, and R. E. Goldstein, Fluid dynamics of bacterial turbulence, Phys. Rev. Lett. **110** (2013) 228102–05.
[9] J. Slomka and J. Dunkel, Generalized Navier-Stokes equations for active suspensions, Euro Phys. J. Special Topics, **224** (2015) 1349–1358.
[10] M. Linkmann, G. Boffetta, M. C. Marchetti, and B. Eckhardt, Phase transition to large scale coherent structures in two-dimensional active matter turbulence, Phys. Rev. Lett. **122** (2019) 214503.
[11] M. Linkmann, M. C. Marchetti, G. Boffetta, and B. Eckhardt, Condensate formation and multiscale dynamics in two-dimensional active suspensions, Phys. Rev. E **101** (2020) 022609–16.
[12] J. Slomka and J. Dunkel, Spontaneous mirror-symmetry breaking induces inverse energy cascade in 3d active fluids, Proc. Nat. Acad. Sci. **114** (2017) 2119–2121.
[13] V. Bratanov, F. Jenko, and E. Frey, New class of turbulence in active fluids, Proc. Nat. Acad. Sci. **112** (2015) 15048–15053.
[14] R. Alert, J. Casademunt, and J.-F. Joanny, Active turbulence, Ann. Rev. Cond. Matter Phys. **13** (2021) 143-170.
[15] M. C. Marchetti, J. F. Joanny, S. Ramaswamy, T. Liverpool, and J. Prost, Hydrodynamics of soft active matter, Rev. Mod. Phys. **85** (2013) 1143–1189.
[16] L. Giomi, Geometry and topology of turbulence in active nematics, Phys. Rev. X **5** (2015) 031003–9.
[17] C. P. Sanjay and A. Joy, Friction scaling laws for transport in active turbulence, Phys. Rev. Fluids, **5** (2020) 024302–9.
[18] S. Mukherjee, R. K. Singh, M. James, S. S. Ray, Anomalous diffusion and Lévy walks distinguish active from inertial turbulence, Phys. Rev. Lett. **127** (2021) 118001–4.
[19] K. V. Kiran, A. Gupta, A. K. Verma, R. Pandit, *Irreversiblity in Bacterial Turbulence: Insights from the Mean-Bacterial-Velocity Model* (2022) arXiv:2201.12722.
[20] J. Swift, P. C. Hohenberg, Hydrodynamic fluctuations at the convective instability, Phys. Rev. A **15** (1977) 319–328 ; M. C. Cross and P. C. Hohenberg, Rev. Mod. Phys., **65**, No. 3, (1993).
[21] N. Rana, P. Perlekar, Coarsening in the two-dimensional incompressible Toner-Tu equation : Signatures of turbulence, Phys. Rev. E **102** (2020) 032617-9.
[22] N. Rana, P. Perlekar, Phase ordering, topological defects, and turbulence in the three-dimensional incompressible Toner-Tu equation, Phys. Rev. E **105** (2022) L032603-6.
[23] L. Chen, C.F. Lee, J. Toner, Mapping two-dimensional polar active fluids to two-dimensional soap and one-dimensional sandblasting, Nature Comm. **7** (2016) 12215-10.
[24] L. Chen, C. F. Lee, J. Toner, Incompressible polar active fluids in the moving phase in dimensions $d > 2$, New J. Phys. **20** (2018) 113035.
[25] M. J. Bowick, N. Fakhri, M. C. Marchetti, S. Ramaswamy, Symmetry, Thermodynamics, and Topology in Active Matter, Phys. Rev. X **12** (2022) 010501-27.
[26] C. Foias, O. Manley, R. Rosa, R. Temam, *Navier-Stokes Equations and Turbulence*, Cambridge University Press (Cambridge 2001).
[27] C. Doering, J. D. Gibbon, *Applied Analysis of the Navier-Stokes equations*, Cambridge University Press (Cambridge 1995).
[28] C. Foias, C. Guillopé, and R. Temam, New apriori estimates for Naviers-Stokes equations in dimension 3, Comm. PDEs **6** (1981) 329–359.
[29] J. D. Gibbon, Weak and strong solutions of the 3D Navier-Stokes equations and their relation to a chessboard of convergent inverse length scales, J. Nonlin. Sci. **29** (2019) 215–228.
[30] J. D. Gibbon, Turbulent cascades and thin sets in 3D Navier-Stokes turbulence, Europhys. Lett. **131** (2020) 64001–05.
[31] F. Zanger, H. Löwen, J. Saal, MNP2015 2015: Math. Nonlin. Phen. – Anal. Comp. (2017) 285—303.
[32] S. Antontsev, H. de Oliveira, The Navier–Stokes problem modified by an absorption term, App. Anal. **89** (2010) 1805–1825.
[33] E. S. Titi, S. Trabelsi, *Global well-posedness of a three-dimensional Brinkman-Forchheimer-Bénard convection model in porous media*, (2022) arXiv:2204.03531v1.
[34] X. Cai, Q. Jiu, Weak and strong solutions for the incompressible Navier–Stokes equations with damping, J. Math.

Anal. App. **343** (2008) 799–809.
[35] A. O. Celebi, V. K. Kalantarov, D. Ugurlu, On continuous dependence on coefficients of the Brinkman–Forchheimer equations, App. Math. Lett. **19** (2006) 801–807.
[36] Y. Liu, C. Lin, Structural stability for Brinkman–Forchheimer equations., Elec. J. Diff. Equs. 2007(02), (2007) 1–8.
[37] M. Louaked, N. Seloula, S. Sun, S. Trabelsi, A pseudocompressibility method for the incompressible Brinkman-Forchheimer equations, Differ. Integral Equ. **28** (2015) 361–382.
[38] M. Louaked, N. Seloula, S. Trabelsi, Approximation of the unsteady Brinkman-Forchheimer equations by the pressure stabilization method, Numer. Meth. PDEs **33** (2017) 1949–1965.
[39] P. A. Markowich, E. S. Titi, S. Trabelsi, Continuous data assimilation for the three-dimensional Brinkman–Forchheimer-extended Darcy model, Nonlinearity **29** (2016) 1292–1328.
[40] L. E. Payne, B. Straughan, Convergence and continuous dependence for the Brinkman–Forchheimer equations, Stud. App. Math. **102** (1999) 419–439.
[41] B. Straughan, *Stability And Wave Motion In Porous Media*, **165**, Springer Science & Business Media (2008).
[42] D. Ugurlu, On the existence of a global attractor for the Brinkman–Forchheimer equations, Nonlin. Anal : Theory, Methods & Applications **68** (2008) 1986–1992.
[43] B. Wang, S. Lin, Existence of global attractors for the three-dimensional Brinkman–Forchheimer equation, Math. Meth. App. Sci. **31** (2008) 1479–1495.
[44] Y. You, C. Zhao, S. Zhou, The existence of uniform attractors for 3d Brinkman–Forchheimer equations, Dis. Cont. Dyn. Sys. A **32** (2012) 787–3800.
[45] D. Donzis, R. M. Kerr, J. D. Gibbon, A. Gupta, R. Pandit, D. Vincenzi, Vorticity moments in four numerical simulations of the 3D Navier-Stokes equations, J. Fluid Mech. **732** (2013) 316–331.
[46] J. D. Gibbon, D. Donzis, R. M. Kerr, A. Gupta, R. Pandit, D. Vincenzi, Regimes of nonlinear depletion and regularity in the 3D Navier-Stokes equations, Nonlinearity **27** (2014) 1–19.
[47] J. D. Gibbon, A. Gupta, G. Krstulovic, R. Pandit, H. Politano, Y. Ponty, A. Pouquet, G. Sahoo, J. Stawarz, Depletion of Nonlinearity in Magnetohydrodynamic Turbulence: Insights from Analysis and Simulations, Phys. Rev. E **93** (2016) 043104.
[48] J. D. Gibbon, A. Gupta, N. Pal, R. Pandit, The role of BKM-type theorems in 3d Euler, Navier-Stokes and Cahn-Hilliard analysis, Physica D : Nonlinear Phenomena **376** (2018) 60–68.
[49] B. Dubrulle, J. D. Gibbon, A correspondence between the multifractal model of turbulence and the Navier–Stokes equations, Phil. Trans. R. Soc. A, **380** (2022) 20210092.
[50] R. A. Adams, *Sobolev Spaces*, Pure and Applied Mathematics, Vol. 65, Academic Press (NY, 1975).
[51] C. Canuto, M. Y. Hussaini, M Yousuff, A. Quarteroni, A. Thomas Jr.,*Spectral methods in fluid dynamics*, Springer Science & Business Media, (2012).
[52] S. M. Cox, P. C. Matthews, Exponential time differencing for stiff systems, J. Comput. Phys., **176** (2002) 430–455.

Supplemental Material

In this Supplemental Material we provide the following additional plots:

1. Illustrative plots for the time series of the total kinetic energy $E_{tot}(t)$, the averaged energy spectrum $E(k)$ (for definitions see below) , and filled contour plots of the vorticity (in $d = 2$) and isosurfaces of the modulus of the vorticity (in $d = 3$).
2. Different norms and their time averages for the temporally frozen states in $d = 2$.
3. In $d = 3$, we plot versus t, $Q_{0,m}$, $Q_{1,m}$, and D_m and their time averages versus m, for a representative run.

Definitions

1. The total kinetic energy per unit volume is
$$E_{tot}(t) = \frac{1}{L^d}\left(\int_{V_d} \frac{\boldsymbol{u}\cdot\boldsymbol{u}}{2}\, dV_d\right).$$
2. The shell-averaged energy spectrum is
$$E(k) = \frac{1}{2}\sum_{k'=k-1/2}^{k'=k+1/2}\sum_{i=1}^{i=d}\left\langle \widetilde{u}_i(\mathbf{k}', t).\widetilde{u}_i(-\mathbf{k}', t)\right\rangle_t ,$$
where $\widetilde{\boldsymbol{u}}(\mathbf{k}, t)$ is the spatial Fourier transform of the velocity field $\boldsymbol{u}(\vec{x}, t)$; $\langle . \rangle_t$ indicates the average over time.
3. Weighted averages of the vorticity are defined as
$$D_m(t) = \|\boldsymbol{\omega}\|_{2m}^{\alpha_{n,m,d=3}} .$$

Supplemental results for two and three dimensions

Run	d	N	δt	ν	α	β
S1	2	2048	2×10^{-4}	6.2×10^{-1}	1	1
S2	2	2048	2×10^{-4}	1.2×10^{-1}	1	1
S3	2	2048	2×10^{-4}	6.0×10^{-2}	1	1
S4	2	2048	2×10^{-4}	3.0×10^{-2}	1	1
S5	2	2048	2×10^{-4}	1.5×10^{-2}	1	1
S6	2	2048	2×10^{-4}	7.0×10^{-3}	1	1
S7	2	2048	2×10^{-4}	3.1×10^{-3}	1	1

Table C.2: The parameters for our DNSs: d is the dimension, N^d the number of collocation points, and δ the time step. For all our runs, $\lambda = 1$.

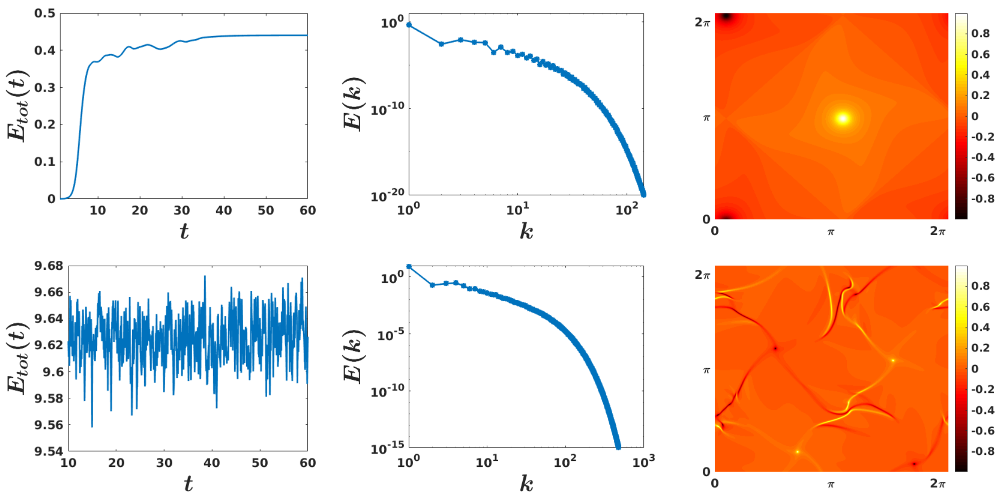

Figure C.5: Plots for runs S7 (row 1) and A6 (row2): column (1) contains plots versus the time t of the total energy $E_{tot}(t)$; column (2) contains log-log plots versus k of the energy spectrum $E(k)$; column (3) comprises filled contour plots of ω at a representative time.

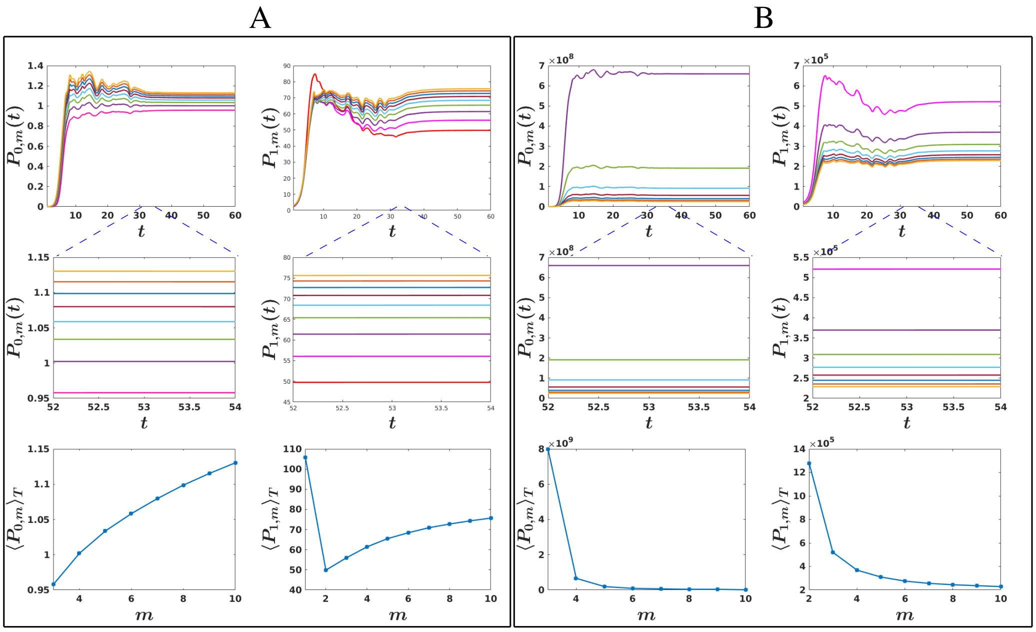

Figure C.6: (Colour online) Illustrative plots for $U_0 = \sqrt{\alpha/\beta}$ (panel A) and $U_0 = \nu/L$ (panel B) for run S7 (see Table C.2): First and second rows: plots versus t of $P_{0,m}$ and $P_{1,m}$; the plots in the second row are expanded versions of small segments of the plots in the first row. Third row: Plots versus m of $\langle P_{0,m}\rangle_T$ and $\langle P_{1,m}\rangle_T$. Curves for $m = 2, 3, 4, 5, 6, 7, 8, 9$, and 10 are drawn in red, pink; violet, green, cyan, maroon, blue, orange, and yellow, respectively.

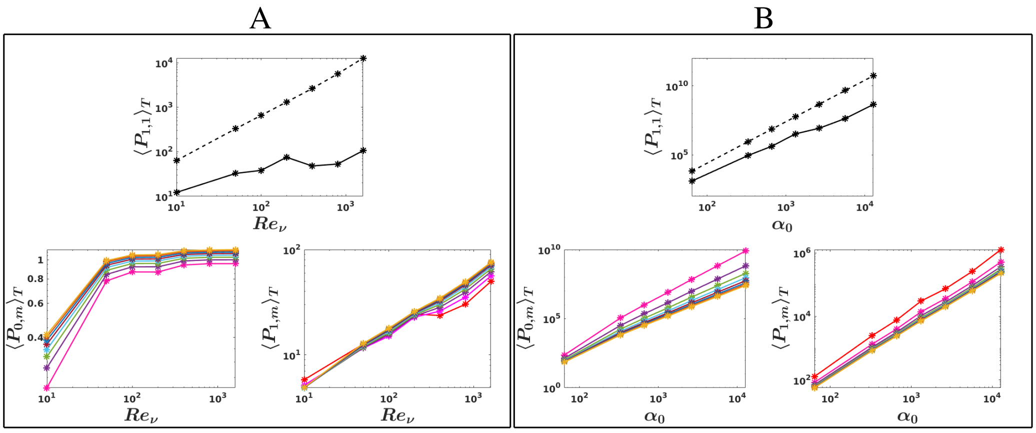

Figure C.7: (Colour online) Illustrative plots for $U_0 = \sqrt{\alpha/\beta}$ (panel A) and $U_0 = \nu/L$ (panel B) for $d = 2$, runs S1-S7 (see Table C.2): First row: plots versus Re_ν (panel A) and α_0 (panel B) of $\langle P_{1,1}\rangle_T$ (solid black line) and $Re_\nu\,\alpha_0\,\mathcal{A}_0$ (dashed black line). Second row: Plots versus Re_ν (panel A) and α_0 (panel B) of $\langle P_{0,m}\rangle_T$ and $\langle P_{1,m}\rangle_T$. Curves for $m = 2, 3, 4, 5, 6, 7, 8, 9$, and 10 are drawn in red, pink; violet, green, cyan, maroon, blue, orange, and yellow, respectively.

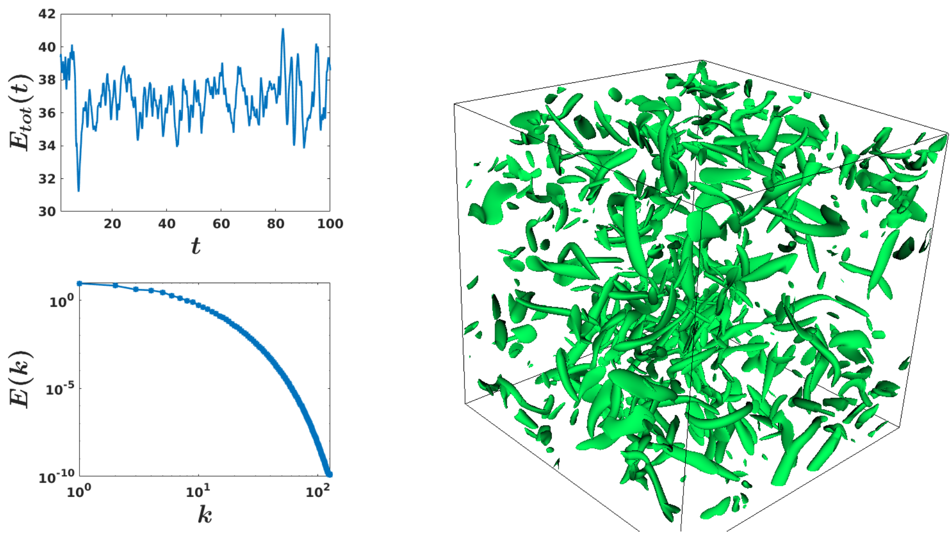

Figure C.8: (Colour online) For run B2; plot versus t of the total kinetic energy $E_{tot}(t)$ (column 1, row 1); log-log plot versus k of the energy spectrum $E(k)$ (column 1, row2); iso-surfaces of the modulus of the vorticity field (column 2).

A

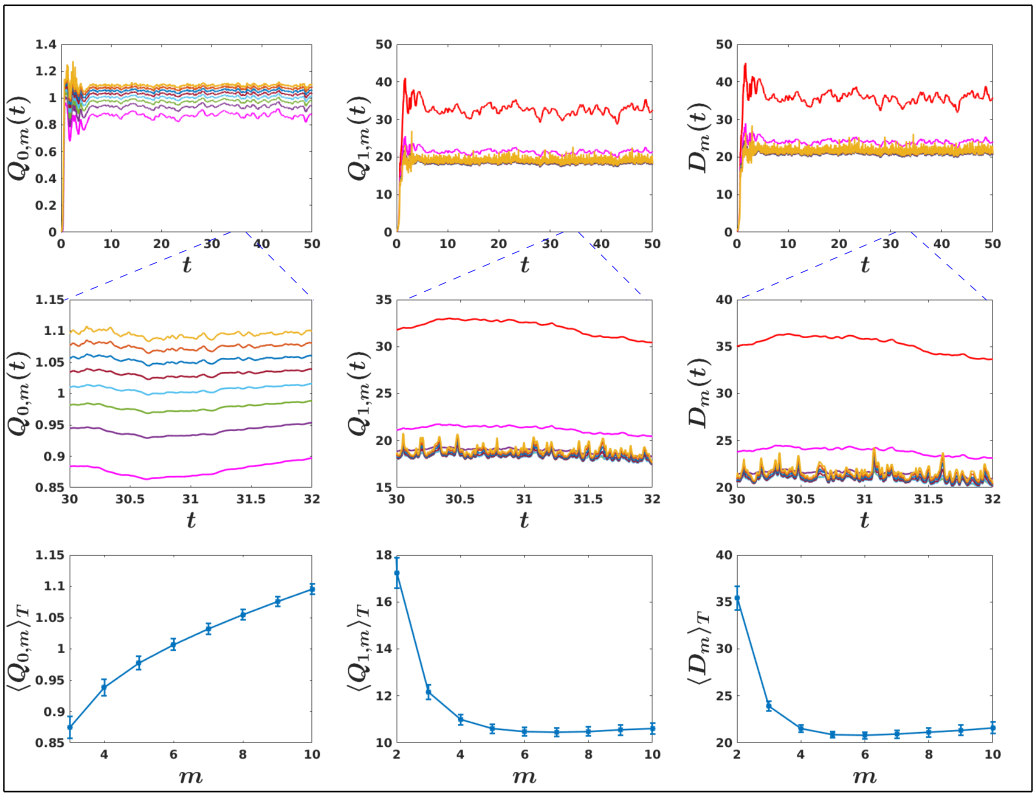

Figure C.9: (Colour online) Illustrative plots for $U_0 = \sqrt{\alpha/\beta}$ (panel A) run B3 (see Table 1, main text): First and second rows : plots versus t of $Q_{0,m}$, $Q_{1,m}$ and D_m ; the plots in the second row are expanded versions of small segments of the plots in the first row. Third row : Plots versus m of $\langle Q_{0,m}\rangle_T$ and $\langle Q_{1,m}\rangle_T$ and $\langle D_m\rangle_T$. Curves for $m = 2, 3, 4, 5, 6, 7, 8, 9,$ and 10 are drawn in red, pink; violet, green, cyan, maroon, blue, orange, and yellow, respectively.

B

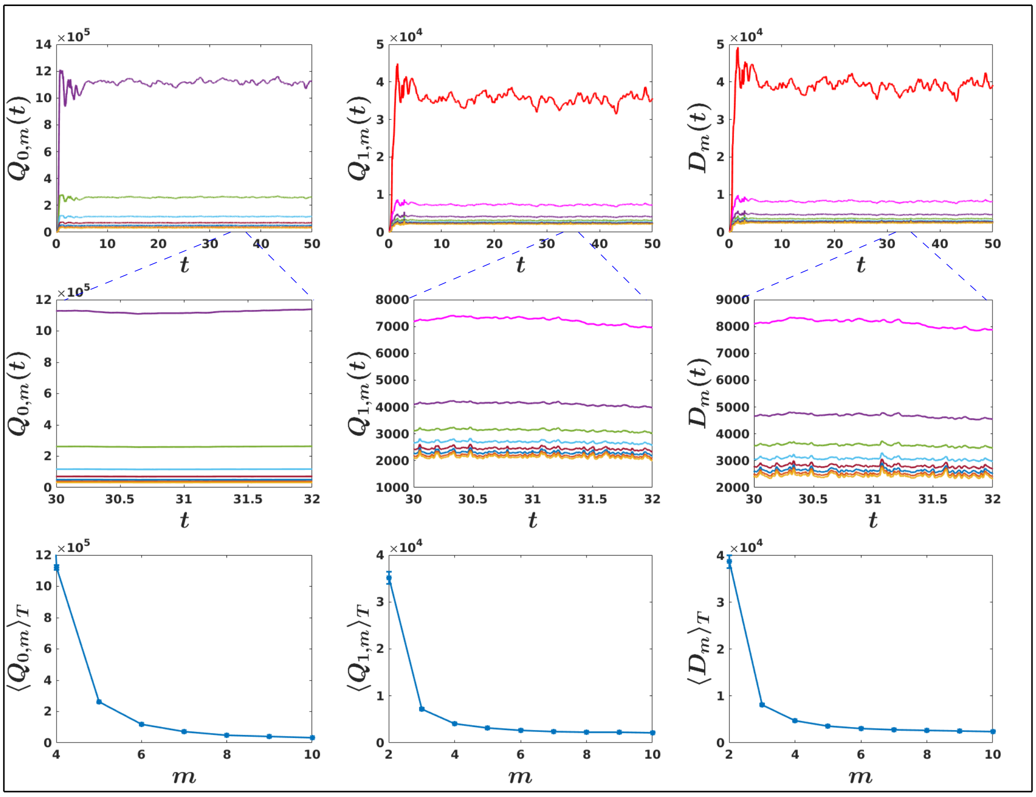

Figure C.10: (Colour online) Illustrative plots for $U_0 = \nu/L$ (panel B) for run B3 (see Table 1, main text): First and second rows : plots versus t of $Q_{0,m}$, $Q_{1,m}$ and D_m ; the plots in the second row are expanded versions of small segments of the plots in the first row. Third row : Plots versus m of $\langle Q_{0,m} \rangle_T$ and $\langle Q_{1,m} \rangle_T$ and $\langle D_m \rangle_T$. Curves for $m = 2, 3, 4, 5, 6, 7, 8, 9,$ and 10 are drawn in red, pink; violet, green, cyan, maroon, blue, orange, and yellow, respectively.